lajss.org© Latin American Journal of Solids and Structures
www.lajss.org

An Efficient Transmitting Boundaries for Seismic Analysis of the Structure-Foundation

Feng Xiong[a*] https://orcid.org/ 0000-0002-2897-1998, Fengqiang Shen[b] https://orcid.org/0000-0001-8696-0149

[a] College of Civil Engineering, Hefei University of Technology, Hefei 230009, China. Email: cvexf@hfut.edu.cn
[b] College of Civil Engineering, Hefei University of Technology, Hefei 230009, China. Email: shenfq@hfut.edu.cn

* Corresponding author

Abstract
The transmitting boundary (TB) is very important for seismic analysis of the structure-foundation. In this paper, the transmitting boundary in the finite element model for seismic analysis of the structure-foundation is studied. First, the modified viscous boundary is developed to address the non-plane wave behavior of the structure-foundation. Then, the seismic analysis of the model for the structure-foundation is formulated, where a potential earthquake is defined by the incoming waves, and the truncated boundary is imposed with the transmitting boundary conditions. Further, the tied boundary model and the transmitting-layer boundary model are set up to address the radiated waves in the model of the structure-foundation. Finally, the transmitting-layer boundary model has been extended for the structure-foundation subject to obliquely and horizontally incoming seismic waves. In comparison with the various schemes of TBs, the proposed transmitting boundaries have advantages of efficiency, convenience and versatility. The research are of great significance for the dynamic response analysis of structural-foundation.

Keywords
seismic wave; transmitting boundary; transmitting-layer boundary model; versatility

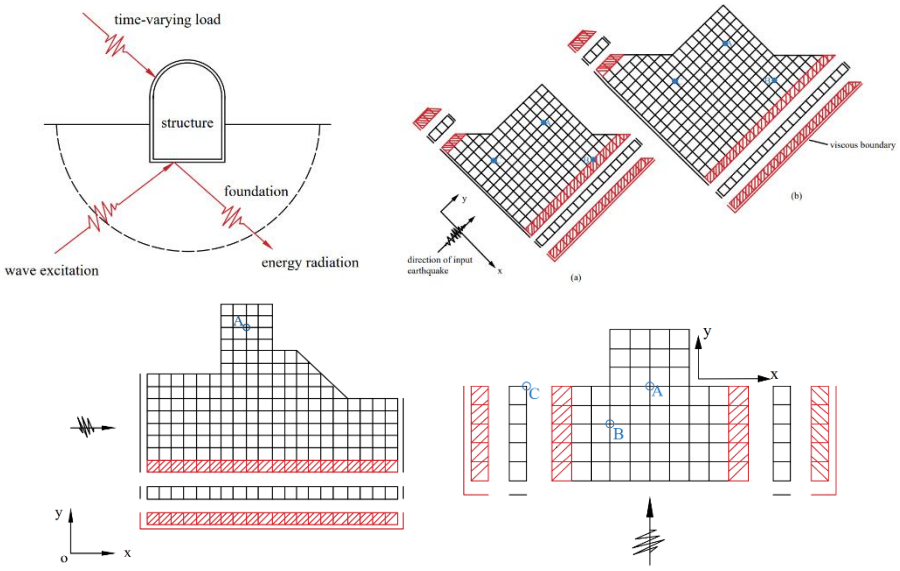

1 INTRODUCTION

The dynamics of the structure-foundation has been studied for over a half century (Shen, 1988; Tirri, 2023; Lysmer and Kuhlemeyer, 1969; Lan and Guo, 2024; Fattah, et al., 2012a), which focuses on determining the stresses and displacements of an engineering structure subject to dynamic loads. The dimensions of engineering structures are finite, so it is easy to select a finite model in space. The finite model in space can be discretized into a discrete system of finite number of degree of freedoms (DOFs). Once the problem is of finite number of DOFs, it can be straightforwardly solved with computer. In general, the structure will interact with its surrounding foundation. The need for analyzing a given structure not as if it were isolated, but rather as a part of the structure-foundation interacting with each other, is making dynamic analysis of the structure-foundation imperative for an increasing range of structures. The structure-foundation problem is an infinite problem, because the foundation is an infinite medium in nature. Computer can only handle finite problems, which means we have to approximate the infinite foundation with a finite model truncated from the infinite one. On the truncated boundary, proper boundary conditions have to be imposed, otherwise the truncated boundary will reflect outgoing waves backwards into the finite model of the structure-foundation.

As for the numerical simulation of seismic response of the structure-foundation, there are two key issues; one of them is how to transmit the outgoing waves out of the computational model while another is how to input the incident seismic waves--vertically upgoing waves, obliquely incoming waves and horizontally incoming waves--into the model at the same time. In other words, the two key issues are strongly related to the artificially truncated boundary and the transmitting boundary conditions imposed on the truncated boundary. The earliest solution to the truncated boundary was to set up truncated boundaries so far away from the structure that the numerical reflections from the truncated boundary, in any time of whole range of numerical simulation, could not reach back into the part of engineering design of the structure and the near field of the foundation. However, this method necessitates a computationally intensive model in space, demands a considerable amount of computer memory, and is time-consuming. Consequently, certain scholars have advocated for a combined model of finite and dynamic infinite elements to effectively absorb outgoing waves (Barros, et al., 2024; Kim and Yun, 2015; Wang, 2024).

Currently, the predominant approach employed involves the establishment of artificial boundaries at the base of the structure-foundation model. These boundaries are designed to permit outgoing waves, originating from the model, to pass through the truncated boundaries without inducing reflections. Based on the fundamental variables used in the formulation of boundary conditions, artificial boundaries are classified into two primary categories: displacement-type and stress-type. For example, the transmitting boundary proposed by Liao et al. (1984) is categorized as a displacement-type boundary. In contrast, the viscous boundary introduced by Lysmer and Kuhlemeyer (1969), the viscoelastic boundary by Liu et al. (2006), and the high-order local time-domain boundaries by Kumar and Kapuria(2022), Chen et al. (2024), and Zhao et al. (2018) are all classified as stress-type boundaries. In recent years, stress-type artificial boundaries have gained widespread adoption and significant advancements due to their high precision and ease of implementation in infinite element software. This trend is well-documented in the works of Farhad and Aydn. (2025), Xu et al. (2012), Chen et al. (2015), Cui et al. (2021) and Xu et al. (2017).

The Free Field Boundary Method (FFBM), introduced by Wolf (1988), was specifically designed for simulating common incident seismic waves in three-dimensional models. This method comprises three interacting components: the main model, absorbing boundaries, and free-field elements. However, the necessary data exchange between these components during each time-step iteration renders the process computationally demanding. Nielsen (2014) later refined the FFBM by integrating the absorbing boundary and free-field elements into a unified entity, aiming to improve efficiency. In contemporary engineering practice, approximate techniques are often preferred for structure-foundation seismic interaction analysis. A prevalent approach, advocated by researchers such as Amorosi and Boldini (2009), Hashash et al. (2010), and Guo et al. (2024), assumes the computational bedrock behaves as a rigid body. This allows seismic waves to be input solely at the bedrock level using displacement or acceleration formulations. Furthermore, lateral boundaries are frequently neglected or treated with simplistic absorbing conditions. Critically, this bedrock rigidity assumption and boundary simplification fundamentally compromise the accuracy of seismic wave propagation simulations along these boundaries, introducing inherent errors into the analysis.

Addressing the need for more accurate boundary conditions, Liu and Lu (1998) pioneered the Wave Method for viscoelastic artificial boundaries. Its core innovation transforms input motion into equivalent loads applied directly at the boundaries, aiming to precisely replicate free-field motion and stress conditions. Subsequent validation studies (e.g., Xia et al.,2025; Pan et al., 2014; Zhang et al., 2014; Bazyar and Song, 2017; Han et al., 2025) have consistently confirmed the Wave Method's effectiveness and accuracy. Building on this foundation, researchers including Huang et al. (2016, 2017), Fattah et al. (2012b) and Fattah et al. (2015) extended the Wave Method's application. They employed it with a

viscoelastic artificial boundary and analytically computed free-field responses to investigate the oblique incidence of seismic waves in homogeneous half-space sites, focusing particularly on the dynamic responses of long, linear tunnels.

While the theoretical foundation of the Wave Method is robust, its practical application in seismic analysis, particularly for three-dimensional structure-foundation systems, is significantly hampered by unresolved computational challenges. A core difficulty lies in the effective computation of equivalent input loads. Accurately determining these loads necessitates precise calculations of both the free-field stresses at truncated boundaries and the additional forces from artificial boundaries. Critically, the accurate quantification of (1) the directional components of these loads across different boundaries and (2) the representative element areas associated with each boundary node remains a complex and demanding task. Consequently, despite the Wave Method's superior accuracy compared to alternative approaches, these persistent computational hurdles—characterized by intricate processing and high computational cost—constitute a significant research gap, limiting its broader practical adoption.

In this paper, based on the basic theory of the wave propagation method, a series of efficient transmitting boundaries have been put forward for seismic analysis of the structure-foundation problem. The validity of the proposed transmitting boundaries is verified by comparing computational results of small models with those of big models under vertically, obliquely and horizontally incident seismic waves.

2 The Finite Element Equations of the Structure-Foundation Problem

The behavior of an engineering structure placed on foundation, shown in Figure 1, subject to any type of dynamic loads, is essentially a phenomenon of wave propagating in the structure and the foundation underlying it. However, due to the complicated geometry of the structure and the irregular distribution of material properties in the structure and the foundation, there exists no general way to express analytically the wave propagation in the structure-foundation in an explicit form. However, using the finite element method to discretize the structure-foundation, the main difficulty mentioned above can be overcome.

The governing equations of dynamics of the structure-foundation (Clough and Penzien, 1975; Zienkiewicz, et al., 2005), with the finite element method in space domain and the finite difference method in time domain, are of following form:

$$[M]\{\ddot{u}\} + [C]\{\dot{u}\} + [K]\{u\} = \{R(t)\} \tag{1}$$

where $[M], [C], [K]$ are the mass, damping, and stiffness matrices; $\{R(t)\}$ is the vector of external nodal force; $\{u\}, \{\dot{u}\}, \{\ddot{u}\}$ are the vectors of the nodal displacement, velocity, and acceleration of the finite element model.

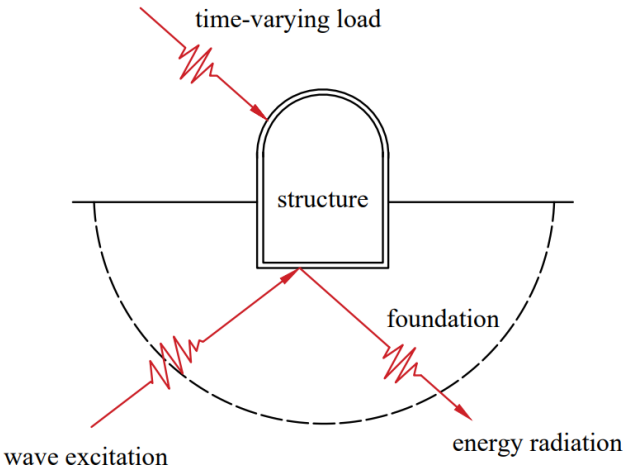

Figure 1 *The structure-foundation problem*

In the problem involving seismic response analysis of structures, the earthquake input mechanism must be considered with special attention because of the interaction of structure and foundation. For relatively small structures, such as resident buildings or water tanks, it is customary to express the earthquake as three mutually orthogonal components of the free field motion. This is the well-known rigid base assumption. However, this assumption is not valid

for large structures like dams, due to the fact that their dynamic response will induce significant interaction effects as a result of their great mass and stiffness, and the motion of the interface as well as the rest of the foundation will differ from the free field motion in an earthquake that would exist without the structure being present. In this case, the rigid base assumption would be difficult to apply for lack of knowledge about the total motion of the foundation perturbed by the structure. This is especially true in the case where no distinct base foundation or base rock exists (Figure 1) and when a truncation of the finite element model has to be chosen arbitrarily. To account for such a case correctly, it is necessary to incorporate proper boundary conditions so that outgoing waves can be transmitted out the boundary while the incoming waves can come into the model. Clearly, if the total motion were to be defined for such a boundary (like in the traditional rigid base approach), no transmitting boundary conditions could be imposed in a simple way. Therefore, it is logical to use the incoming wave as the earthquake input. In this way the dynamic interaction of the structure-foundation system can be addressed consistently with the model.

The nodes of the finite element model consist of the truncated boundary nodes *B* and the remaining interior nodes *I*. The equations of motion (1) can be partitioned into following form.

$$\begin{bmatrix} M^{II} & M^{IB} \\ M^{BI} & M^{BB} \end{bmatrix} \begin{Bmatrix} \ddot{u}^I \\ \ddot{u}^B \end{Bmatrix} + \begin{bmatrix} C^{II} & C^{IB} \\ C^{BI} & C^{BB} \end{bmatrix} \begin{Bmatrix} \dot{u}^I \\ \dot{u}^B \end{Bmatrix} + \begin{bmatrix} 0 & 0 \\ 0 & c_t^{BB} \end{bmatrix} \begin{Bmatrix} 0 \\ \dot{u}^B \end{Bmatrix} + \begin{bmatrix} K^{II} & K^{IB} \\ K^{BI} & K^{BB} \end{bmatrix} \begin{Bmatrix} u^I \\ u^B \end{Bmatrix} + \begin{bmatrix} 0 & 0 \\ 0 & k_t^{BB} \end{bmatrix} \begin{Bmatrix} 0 \\ u^B \end{Bmatrix} = \begin{Bmatrix} R^I(t) \\ R^B(t) \end{Bmatrix} \tag{2}$$

in which, c_t^{BB} and k_t^{BB} are the damping and spring matrices related to the transmitting boundary conditions.

The total motion u can be split into the reference motion $a_{i0}(t)$ (the incoming waves on the truncated boundary) and the relative motion u_r.

$$\begin{Bmatrix} \ddot{u}^I \\ \ddot{u}^B \end{Bmatrix} = \begin{Bmatrix} \ddot{u}_r^I \\ \ddot{u}_r^B \end{Bmatrix} + I_x \ddot{a}_{i0}^x(t) + I_y \ddot{a}_{i0}^y(t) + I_z \ddot{a}_{i0}^z(t)$$

(3a)

$$\begin{Bmatrix} \dot{u}^I \\ \dot{u}^B \end{Bmatrix} = \begin{Bmatrix} \dot{u}_r^I \\ \dot{u}_r^B \end{Bmatrix} + I_x \dot{a}_{i0}^x(t) + I_y \dot{a}_{i0}^y(t) + I_z \dot{a}_{i0}^z(t)$$

(3b)

$$\begin{Bmatrix} u^I \\ u^B \end{Bmatrix} = \begin{Bmatrix} u_r^I \\ u_r^B \end{Bmatrix} + I_x a_{i0}^x(t) + I_y a_{i0}^y(t) + I_z a_{i0}^z(t)$$

(3c)

where

$$I_x = (1 \quad 0 \quad 0 \quad \cdots \quad 1 \quad 0 \quad 0 \quad \cdots \quad 1 \quad 0 \quad 0)^T$$

(4a)

$$I_y = (0 \quad 1 \quad 0 \quad \cdots \quad 0 \quad 1 \quad 0 \quad \cdots \quad 0 \quad 1 \quad 0)^T$$

(4b)

$$I_z = (0 \quad 0 \quad 1 \quad \cdots \quad 0 \quad 0 \quad 1 \quad \cdots \quad 0 \quad 0 \quad 1)^T$$

(4c)

Therefore Eq. (2) can be reformulated in terms of relative motion.

$$\begin{bmatrix} M^{II} & M^{IB} \\ M^{BI} & M^{BB} \end{bmatrix} \begin{Bmatrix} \ddot{u}_r^I \\ \ddot{u}_r^B \end{Bmatrix} + \begin{bmatrix} C^{II} & C^{IB} \\ C^{BI} & C^{BB} + c_t^{BB} \end{bmatrix} \begin{Bmatrix} \dot{u}_r^I \\ \dot{u}_r^B \end{Bmatrix} + \begin{bmatrix} K^{II} & K^{IB} \\ K^{BI} & K^{BB} + k_t^{BB} \end{bmatrix} \begin{Bmatrix} u_r^I \\ u_r^B \end{Bmatrix} = \begin{Bmatrix} R^I(t) \\ R^B(t) \end{Bmatrix} - \begin{bmatrix} M^{II} & M^{IB} \\ M^{BI} & M^{BB} \end{bmatrix} \{ I_x \ddot{a}_{i0}^x(t) +$$

$$I_y \ddot{a}_{i0}^y(t) + I_z \ddot{a}_{i0}^z(t) \} - \begin{bmatrix} 0 & 0 \\ 0 & c_t^{BB} \end{bmatrix} \{ I_x \dot{a}_{i0}^x(t) + I_y \dot{a}_{i0}^y(t) + I_z \dot{a}_{i0}^z(t) \} \tag{5}$$

The explicit-implicit algorithm of the Newmark method is usually adopted for the integral of Eq. (5). For nodes on the truncated boundary the explicit formulas are

$$\{\dot{u}_r^B\}_{n+1} = \{\dot{u}_r^B\}_n + \frac{1}{2}\Delta t(\{\ddot{u}_r^B\}_n + \{\ddot{u}_r^B\}_{n+1})$$
(6a)
$$\{u_r^B\}_{n+1} = \{u_r^B\}_n + \Delta t\{\dot{u}_r^B\}_n + \frac{1}{2}\Delta t^2\{\ddot{u}_r^B\}$$
(6b)

For the remaining interior nodes, the implicit formulas are
$$\{\dot{u}_r^I\}_{n+1} = \{\dot{u}_r^I\}_n + \Delta t(1-\gamma)\{\ddot{u}_r^I\}_n + \Delta t\gamma\{\ddot{u}_r^I\}_{n+1}$$
(7a)
$$\{\mathrm{u}_\mathrm{r}^\mathrm{I}\}_{\mathrm{n}+1} = \{\mathrm{u}_\mathrm{r}^\mathrm{I}\}_\mathrm{n} + \Delta\mathrm{t}\{\dot{\mathrm{u}}_\mathrm{r}^\mathrm{I}\}_\mathrm{n} + \frac{1}{2}\Delta\mathrm{t}^2(1-2\beta)\{\ddot{\mathrm{u}}_\mathrm{r}^\mathrm{I}\}_\mathrm{n} + \beta\Delta\mathrm{t}^2\{\ddot{\mathrm{u}}_\mathrm{r}^\mathrm{I}\}_{\mathrm{n}+1}$$
(7b)

3 Non-plane Waves and The Modified Viscous Boundary Conditions

Without loss of generality (Shen, 1988; Zienkiewicz, et al., 1989), let us suppose a train of non-plane waves propagating in x direction (Figure 2), i.e.
$$u = u(x - c_1 t, y, z)$$
(8a)
$$v = v(x - c_2 t, y, z)$$
(8b)
$$w = w(x - c_2 t, y, z)$$
(8c)

We have normal derivatives of displacements u, v, w in terms of particle velocities $\dot{u}, \dot{v}, \dot{w}$.
$$\frac{\partial u}{\partial x} = -\frac{1}{c_1}\dot{u}$$
(9a)
$$\frac{\partial v}{\partial x} = -\frac{1}{c_2}\dot{v}$$
(9b)
$$\frac{\partial w}{\partial x} = -\frac{1}{c_2}\dot{w}$$
(9c)

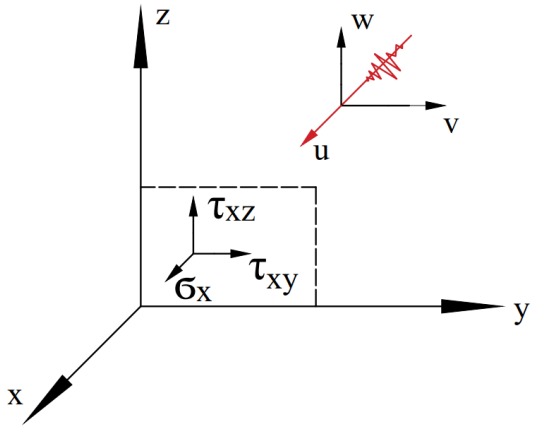

Figure 2 *Wave propagation in x direction*

The corresponding strain components are derived as follows.
$$\varepsilon_x = \frac{\partial u}{\partial x} = -\frac{1}{c_1}\dot{u}$$
(10a)
$$\varepsilon_y = \frac{\partial v}{\partial y}$$
(10b)
$$\varepsilon_z = \frac{\partial w}{\partial z}$$
(10c)
$$\gamma_{xy} = \frac{\partial u}{\partial y} + \frac{\partial v}{\partial x} = \frac{\partial u}{\partial y} - \frac{1}{c_2}\dot{v}$$
(10d)

$$\gamma_{yz} = \frac{\partial v}{\partial z} + \frac{\partial w}{\partial y} \tag{10e}$$

$$\gamma_{zx} = \frac{\partial w}{\partial x} + \frac{\partial u}{\partial z} = \frac{\partial u}{\partial z} - \frac{1}{c_2}\dot{w} \tag{10f}$$

Therefore, the stress components $\sigma_x, \tau_{xy}, \tau_{xz}$on the truncated boundary can be expressed in terms of displacement derivatives as follows.

$$\sigma_x = -\rho c_1 \dot{u} + \rho(c_1^2 - 2c_2^2)\frac{\partial v}{\partial y} + \rho(c_1^2 - 2c_2^2)\frac{\partial w}{\partial z} \tag{11a}$$

$$\tau_{xy} = -\rho c_2 \dot{v} + \rho c_2^2 \frac{\partial u}{\partial y} \tag{11b}$$

$$\tau_{xz} = -\rho c_2 \dot{w} + \rho c_2^2 \frac{\partial u}{\partial z} \tag{11c}$$

where ρ is the material density, c_1 and c_2 are pressure and shear wave speeds, respectively. Their relationships with the Yong's modulus E and Poisson's ratio μ are shown as follows.

$$c_1 = \sqrt{\frac{(1-\mu)E}{(1+\mu)(1-2\mu)}} \tag{12a}$$

$$c_2 = \sqrt{\frac{E}{2(1+\mu)}} \tag{12b}$$

These are the modified viscous boundary conditions. They include the standard viscous boundary conditions as a special case if waves are purely plane ones. It is reasonable to anticipate that the modified viscous boundary conditions developed here will perform better than the standard viscous boundary in practical computations where waves generally do not propagate purely in a plane manner.

4 Numerical Implementation of the Modified Viscous Boundary Conditions

For a finite model with a truncated boundary in 2-D (Figure 3), the modified viscous boundary conditions can be written down as follows.

$$p_\xi = -\rho c_1 \dot{u}_\xi + \rho(c_1^2 - 2c_2^2)\frac{\partial u_\eta}{\partial \eta} \tag{13a}$$

$$p_\eta = -\rho c_2 \dot{u}_\eta + \rho c_2^2 \frac{\partial u_\xi}{\partial \eta} \tag{13b}$$

where p, u and $\dot{u}$ stand for the traction, the displacement and the velocity, respectively; ξ, η are the local coordinates in the outer normal and the tangential directions, respectively.

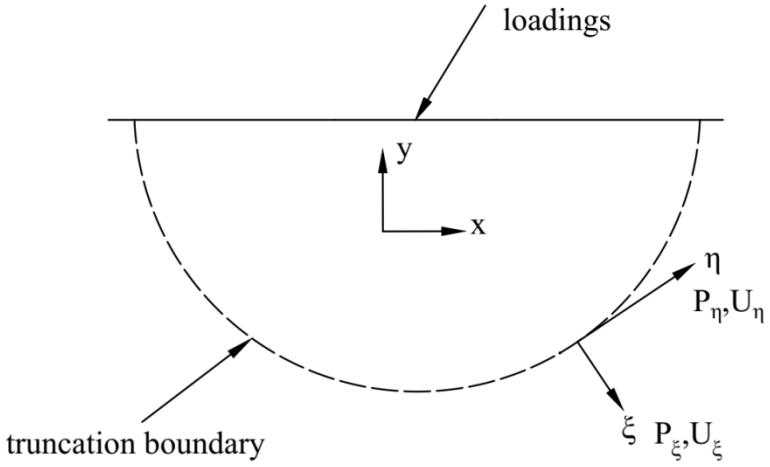

Figure 3 *A Finite Model with The Transmitting Boundary*

The transmitting boundary can be discretized into a line element mesh (Figure 4), and the transmitting boundary conditions (13) will be imposed in a similar way as the usual traction boundary conditions.

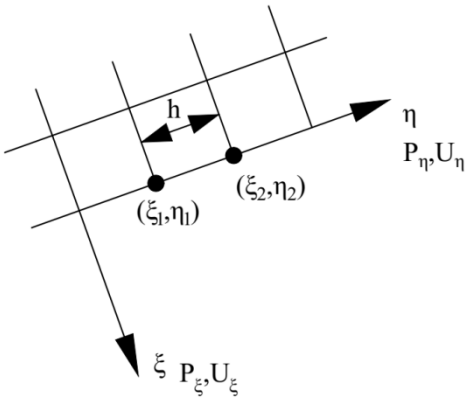

***Figure** 4 The Truncated Boundary and Finite Element Discretization*

For a typical line element e on the truncated boundary as shown in Figure 4, its potential energy contributed by the boundary conditions (13) is as follows.

$$\delta w^e = \int_{\eta_1}^{\eta_2} [\delta u_\xi \quad \delta u_\eta] \begin{Bmatrix} p_\xi \\ p_\eta \end{Bmatrix} d\eta \tag{14}$$

Substituting Equations (13) into Equation (14), it is found that

$$\delta w^e = -\int_{\eta_1}^{\eta_2} [\delta u_\xi \quad \delta u_\eta] \begin{bmatrix} \rho c_1 & 0 \\ 0 & \rho c_2 \end{bmatrix} \begin{Bmatrix} \dot{u}_\xi \\ \dot{u}_\eta \end{Bmatrix} d\eta - \int_{\eta_1}^{\eta_2} [\delta u_\xi \quad \delta u_\eta] \begin{bmatrix} 0 & -\rho(c_1^2 - 2c_2^2) \\ -\rho c_2^2 & 0 \end{bmatrix} \frac{\partial}{\partial \eta} \begin{Bmatrix} u_\xi \\ u_\eta \end{Bmatrix} d\eta \tag{15}$$

Inside a line boundary element, it is assumed that

$$\begin{Bmatrix} u_\xi \\ u_\eta \end{Bmatrix} = \begin{bmatrix} \underline{N} & 0 \\ 0 & \underline{N} \end{bmatrix} \begin{Bmatrix} \underline{u}_\xi \\ \underline{u}_\eta \end{Bmatrix} \tag{16a}$$

$$\begin{Bmatrix} \dot{u}_\xi \\ \dot{u}_\eta \end{Bmatrix} = \begin{bmatrix} \underline{N} & 0 \\ 0 & \underline{N} \end{bmatrix} \begin{Bmatrix} \dot{\underline{u}}_\xi \\ \dot{\underline{u}}_\eta \end{Bmatrix} \tag{16b}$$

$\left[\underline{N}\right]$ is the matrix of shape functions

$$\left[\underline{N}\right] \equiv [N_1 \quad N_2] \equiv \left[1 - \frac{\eta}{h} \quad \frac{\eta}{h}\right] \tag{17}$$

h is the length of the boundary element (shown in the Figure 4). And $\{\underline{u}\}$ denotes the vector of nodal displacement.

$$\{\underline{u}\} \equiv \begin{Bmatrix} \underline{u}_\xi \\ \underline{u}_\eta \end{Bmatrix} \equiv \begin{Bmatrix} u_{1\xi} \\ u_{2\xi} \\ u_{1\eta} \\ u_{2\eta} \end{Bmatrix} \tag{18}$$

And $\{\dot{\underline{u}}\}$ denotes the vector of nodal velocity.

$$\{\dot{\underline{u}}\} \equiv \begin{Bmatrix} \dot{\underline{u}}_\xi \\ \dot{\underline{u}}_\eta \end{Bmatrix} \equiv \begin{Bmatrix} \dot{u}_{1\xi} \\ \dot{u}_{2\xi} \\ \dot{u}_{1\eta} \\ \dot{u}_{2\eta} \end{Bmatrix} \tag{19}$$

Therefore,

$$\begin{Bmatrix} \delta u_\xi \\ \delta u_\eta \end{Bmatrix} = \begin{bmatrix} \underline{N} & 0 \\ 0 & \underline{N} \end{bmatrix} \begin{Bmatrix} \delta \underline{u}_\xi \\ \delta \underline{u}_\eta \end{Bmatrix} \tag{20}$$

$$\frac{\partial}{\partial\eta}\begin{Bmatrix}u_\xi\\u_\eta\end{Bmatrix}=\frac{\partial}{\partial\eta}\begin{bmatrix}\underline{N}&0\\0&\underline{N}\end{bmatrix}\begin{Bmatrix}\underline{u}_\xi\\\underline{u}_\eta\end{Bmatrix}$$

(20)

Define

$$[c_t]\equiv\int_{\eta_1}^{\eta_2}\begin{bmatrix}\underline{N}^T&0\\0&\underline{N}^T\end{bmatrix}\begin{bmatrix}\rho c_1&0\\0&\rho c_2\end{bmatrix}\begin{bmatrix}\underline{N}&0\\0&\underline{N}\end{bmatrix}d\eta$$

(21)

$$[k_t]\equiv\int_{\eta_1}^{\eta_2}\begin{bmatrix}\underline{N}^T&0\\0&\underline{N}^T\end{bmatrix}\begin{bmatrix}0&-\rho(c_1^2-2c_2^2)\\-\rho c_2^2&0\end{bmatrix}\frac{\partial}{\partial\eta}\begin{bmatrix}\underline{N}&0\\0&\underline{N}\end{bmatrix}d\eta$$

(22)

where $[c_t]$ is the damping matrix due to the viscous boundary conditions, and $[k_t]$ is the stiffness-like matrix contributed by the modified boundary conditions. With these definitions, Eq. (15) can be reduced into

$$\delta w^e=-\begin{bmatrix}\delta\underline{u}_\xi^T&\delta\underline{u}_\eta^T\end{bmatrix}[c_t]\begin{Bmatrix}\dot{\underline{u}}_\xi\\\dot{\underline{u}}_\eta\end{Bmatrix}-\begin{bmatrix}\delta\underline{u}_\xi^T&\delta\underline{u}_\eta^T\end{bmatrix}[k_t]\begin{Bmatrix}\underline{u}_\xi\\\underline{u}_\eta\end{Bmatrix}$$

(23)

where the vector of nodal forces related to the transmitting boundary conditions is defined as follows.

$$\{\underline{P}\}=-[c_t]\{\dot{\underline{u}}\}-[k_t]\{\underline{u}\}$$

(24)

And

$$\{\underline{P}\}=\begin{Bmatrix}\underline{P}_\xi\\\underline{P}_\xi\end{Bmatrix}=\begin{Bmatrix}P_{1\xi}\\P_{2\xi}\\P_{1\eta}\\P_{2\eta}\end{Bmatrix}$$

(25)

The standard viscous boundary can be implemented in the same way by letting

$$[k_t]=0$$

(26)

The damping matrix $[c_t]$ and the stiffness-like matrix $[k_t]$ assume following values

$$[c_t]\equiv\begin{bmatrix}2d_1&d_1&0&0\\d_1&2d_1&0&0\\0&0&2d_2&d_2\\0&0&d_2&2d_2\end{bmatrix}$$

(27)

$$[k_t]\equiv\begin{bmatrix}0&0&k_1&-k_1\\0&0&k_1&-k_1\\k_2&-k_2&0&0\\k_2&-k_2&0&0\end{bmatrix}$$

(28)

in which,

$$d_1=\frac{1}{6}\rho c_1 h$$

(29a)

$$d_2=\frac{1}{6}\rho c_2 h$$

(29b)

$$k_1=\frac{1}{2}\rho(c_1^2-2c_2^2)$$

(29c)

$$k_2=\frac{1}{2}\rho c_2^2$$

(29d)

It should be pointed out that in practical computation with explicit algorithm the damping matrix $[c_t]$ has to be lumped into a diagonal matrix.

$$[c_t'] \equiv \begin{bmatrix} 3d_1 & 0 & 0 & 0 \\ 0 & 3d_1 & 0 & 0 \\ 0 & 0 & 3d_2 & 0 \\ 0 & 0 & 0 & 3d_2 \end{bmatrix} \quad (30)$$

5 Models of the Structure-Foundation for Seismic Analysis

5.1 The Tied Boundary Model

5.1.1 A Periodically Spaced Structure-foundation

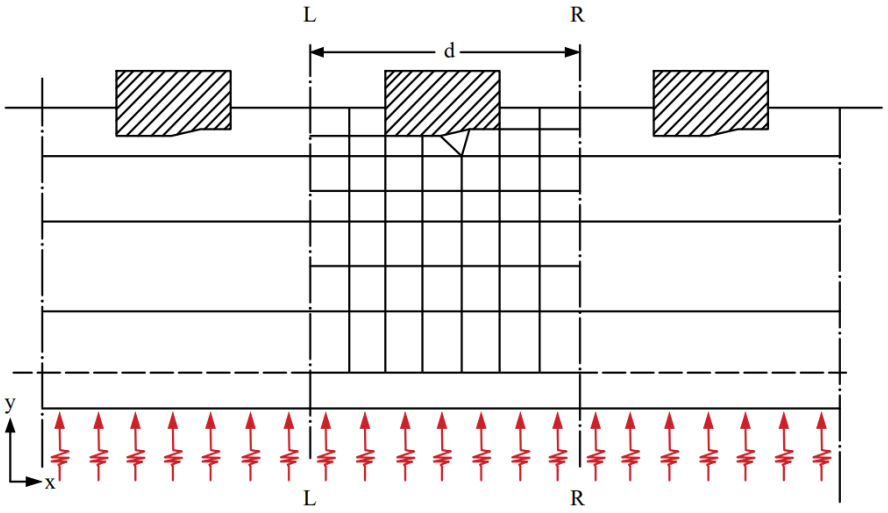

Figure 5 *A Periodically Spaced Structure-Foundation Subject to Seismic Waves*

Consider the periodically spaced structure-foundation system shown in *Figure* 5, where the symmetric lines L-L and R-R define the elementary repeatable domain. The periodical length in horizontal direction is *d*. This means that the geometrical and mechanical properties are invariant under any horizontal translation with a distance d. It can be shown that the motion of periodically spaced system will be periodical in horizontal direction if the loading or the input seismic waves are also periodical in horizontal direction. This is clearly the case when the periodically spaced structure-foundation is subjected to vertically upgoing seismic waves. Therefore, once the motion in the domain between a pair of symmetric lines L-L and R-R with distance *d* is known, the motion of the whole system can be obtained by following translation, i.e.

$$a(x+d,y) = a(x,y) \quad (31a)$$

$$a(x-d,y) = a(x,y) \quad (31b)$$

where a stands for any kinematic or dynamic variable of the structure-foundation problem, and the same relationship also hold for corresponding field derivatives.

The finite element model with the transmitting boundary for seismic analysis can be chosen as shown in Figure 6. The validity of this model can be tested by comparisons of the results between the models truncated at different positions in depth.

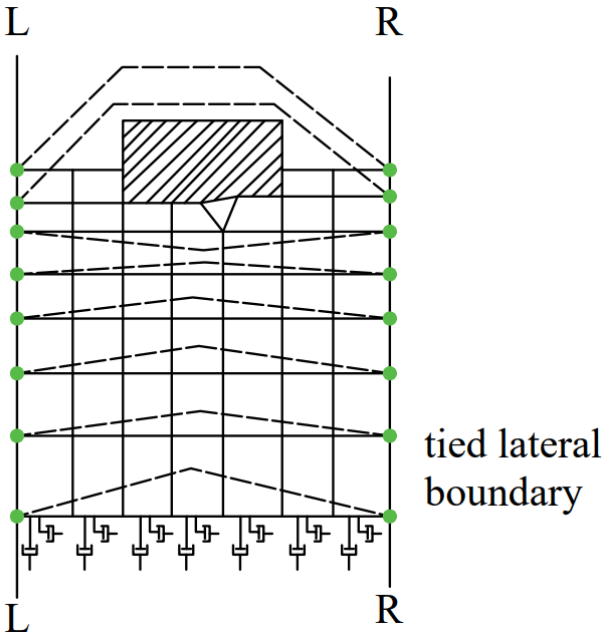

Figure 6 *The Model of the Periodically Spaced Structure-Foundation*

5.1.2 Treatment of Lateral Boundary

For a periodically spaced structure-foundation problem, the lateral boundaries of the model are truncated along the symmetric lines L-L and R-R. The lateral boundary conditions are that the motions of correspondent nodes on the lateral boundaries are identical. These conditions can be imposed by substitution of the unknowns on one side boundary into the ones on the other side boundary (Figure 6). In other words, the corresponding nodes on both lateral boundaries are tied together. This is why that this treatment of the lateral boundary is also called the tied boundary model.

5.1.3 Treatment of Bottom Boundary

Either the standard viscous boundary or the modified viscous boundary can be adopted for the truncated bottom boundary. It is assumed that all nodes on the bottom boundary assume the same incident seismic waves, and the outgoing waves on the bottom nodes can assume different values at different nodes.

This periodical model is fully applicable to the nonlinear dynamic analysis. It leaves the flexibility of choice of explicit or implicit algorithm in time marching. The only requirement is that the linear material behavior has to be maintained in the foundation-layer immediately adjacent to the truncated boundary.

5.2 The Transmitting-Layer Boundary Model

5.2.1 Basics

For a 2-D structure-foundation problem, two boundary models have been developed in present study to fulfil the task of transmitting outgoing waves. The first one is the tied boundary model and it approximates the non-periodical structure-foundation with the model of periodically spaced structure-foundation. However, this model is difficult to apply for the irregular near-field conditions where the two sides of the foundation are at different levels and when the incident waves are input obliquely into the structure-foundation. In order to overcome the difficulty, a transmitting-layer boundary model has been developed to transmit laterally outgoing waves.

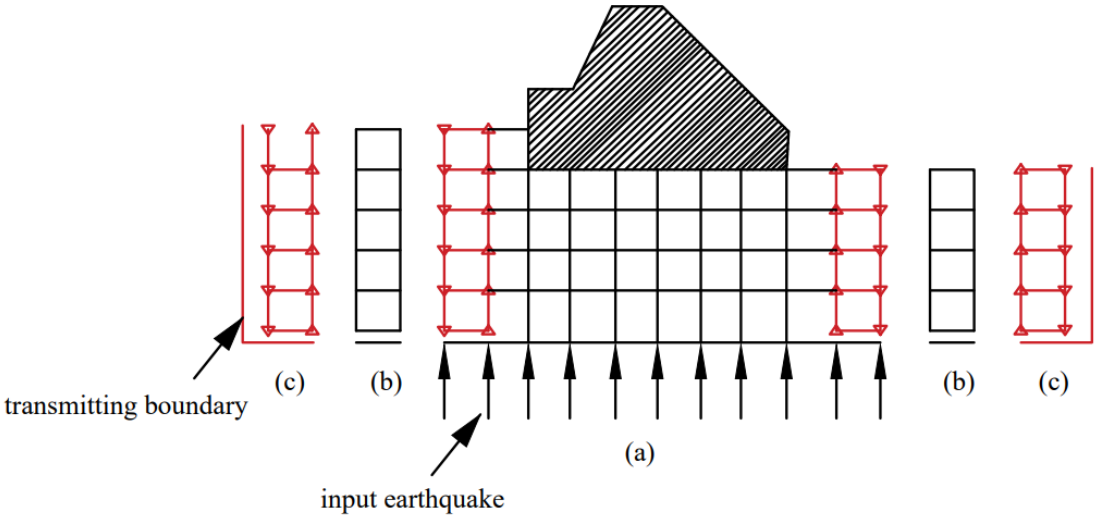

(a)the main mesh (b)the free-field columns (c)the transmitting-layers

Figure7 *The Transmitting-Layer Model*

The transmitting-layer boundary model (Figure 7) is conceptually composed of three parts: Main mesh – degrees of freedom u_r; Free-field column – degrees of freedom u_{fr}; Transmitting-layer – degrees of freedom u_o.

It is clear that the motion of the foundation with the structure attached to it will differ from the free-field motion. This difference in the foundation a distance away from the perturbation is that the waves going out of the main mesh. So, the outgoing waves on the lateral boundary can be obtained as the difference between the motion in main mesh u_r and the motion in free-field column u_{fr}, i.e.

$$u_o = u_r - u_{fr} \tag{32}$$

Therefore, it is the different motion between the main mesh and the free-field that should be imposed with the transmitting boundary conditions at the lateral boundary L-L and R-R.

5.2.2 Main mesh

The governing equations for the main mesh are as follows.

$$\begin{bmatrix} M^{II} & 0 \\ 0 & M_d^{BB} \end{bmatrix}_m \begin{Bmatrix} \ddot{u}_r^I \\ \ddot{u}_r^B \end{Bmatrix}_m + \begin{bmatrix} C^{II} & 0 \\ 0 & C_d^{BB} + c_{t\_d}^{BB} \end{bmatrix}_m \begin{Bmatrix} \dot{u}_r^I \\ \dot{u}_r^B \end{Bmatrix}_m + \begin{bmatrix} K^{II} & K^{IB} \\ K^{BI} & K^{BB} + k_t^{BB} \end{bmatrix}_m \begin{Bmatrix} u_r^I \\ u_r^B \end{Bmatrix}_m = \begin{Bmatrix} R^I(t) \\ R^B(t) \end{Bmatrix}_m -$$
$$\begin{bmatrix} M^{II} & 0 \\ 0 & M_d^{BB} \end{bmatrix}_m \left\{ I_x \ddot{a}_{i0}^x(t) + I_y \ddot{a}_{i0}^y(t) \right\} - \begin{bmatrix} 0 & 0 \\ 0 & c_{t_d}^{BB} \end{bmatrix}_m \left\{ I_x \dot{a}_{i0}^x(t) + I_y \dot{a}_{i0}^y(t) \right\} \tag{33}$$

The subscript *m* stands for the matrices of the main mesh. The unknowns are as follows.

$$\begin{Bmatrix} u_r^I \\ u_r^B \end{Bmatrix}_m, \begin{Bmatrix} \dot{u}_r^I \\ \dot{u}_r^B \end{Bmatrix}_m, \begin{Bmatrix} \ddot{u}_r^I \\ \ddot{u}_r^B \end{Bmatrix}_m \tag{34}$$

In this formulation, they are the displacement, velocity and acceleration of the structure-foundation relative to the incoming waves $\{a_{i0}\}, \{\dot{a}_{i0}\}, \{\ddot{a}_{i0}\}$ on the truncated bottom boundary.

It should be noted that values of the relative motion on the lateral boundary L-L and R-R are never solved from the governing equations of the main mesh as they are always obtained by combining the solution of the free-field column and the solution of the transmitting-layer. It means that all the values of the motion on the lateral boundary of the main mesh are specified in the process of time integral of the governing equations of the main mesh. The solution of the main mesh can be carried out by the mixed algorithm of Newmark method with explicit one for the truncated boundary nodes and implicit one for the remaining interior nodes.

5.2.3 Free-field column

The governing equations of the free-field column are actually a 1-D formulated with a column of 2-D finite element mesh.

$$\begin{bmatrix} M^{II} & 0 \\ 0 & M_d^{BB} \end{bmatrix}_f \begin{Bmatrix} \ddot{u}_r^I \\ \ddot{u}_r^B \end{Bmatrix}_f + \begin{bmatrix} 0 & 0 \\ 0 & c_{t\_d}^{BB} \end{bmatrix}_f \begin{Bmatrix} \dot{u}_r^I \\ \dot{u}_r^B \end{Bmatrix}_f + \begin{bmatrix} K^{II} & K^{IB} \\ K^{BI} & K^{BB} + k_t^{BB} \end{bmatrix}_f \begin{Bmatrix} u_r^I \\ u_r^B \end{Bmatrix}_f = -\begin{bmatrix} M^{II} & 0 \\ 0 & M_d^{BB} \end{bmatrix}_f \left\{ I_x \ddot{a}_{i0}^x(t) + I_y \ddot{a}_{i0}^y(t) \right\} - \begin{bmatrix} 0 & 0 \\ 0 & c_{t\_d}^{BB} \end{bmatrix}_f \left\{ I_x \dot{a}_{i0}^x(t) + I_y \dot{a}_{i0}^y(t) \right\} \tag{35}$$

The subscript *f* stands for the free-field column, and the material damping is neglected. The unknowns of the above equations are the relative nodal displacement, velocity and acceleration of the free-field column to the incoming wave on the truncated bottom boundary. The nodes on the two laterally truncated boundary are tied together in the same way as the treatment of the laterally truncated boundary of the periodically spaced problem.

The solution of the free-field column is carried out with the explicit algorithm of Newmark method.

5.2.4 Transmitting-layer

Physically the transmitting-layer could be visualized as a layer of finite elements neighboring to the lateral boundary of the main mesh. It is used to transmit outgoing waves in the main mesh. Therefore, the governing equations of the transmitting-layer are essentially homogeneous wave equations. The discretized governing equations are

$$\begin{bmatrix} M^{II} & 0 \\ 0 & M_d^{BB} \end{bmatrix}_l \begin{Bmatrix} \ddot{u}_o^I \\ \ddot{u}_o^B \end{Bmatrix}_l + \begin{bmatrix} 0 & 0 \\ 0 & c_{t\_d}^{BB} \end{bmatrix}_l \begin{Bmatrix} \dot{u}_o^I \\ \dot{u}_o^B \end{Bmatrix}_l + \begin{bmatrix} K^{II} & K^{IB} \\ K^{BI} & K^{BB} + k_t^{BB} \end{bmatrix}_l \begin{Bmatrix} u_o^I \\ u_o^B \end{Bmatrix}_l = 0 \tag{36}$$

In which the subscript *l* denotes the transmitting-layer, and the unknowns are

$$\begin{Bmatrix} u_o^I \\ u_o^B \end{Bmatrix}_l \equiv \begin{Bmatrix} u_o^{b1} \\ u_o^{b2} \end{Bmatrix}_l, \begin{Bmatrix} \dot{u}_o^I \\ \dot{u}_o^B \end{Bmatrix}_l \equiv \begin{Bmatrix} \dot{u}_o^{b1} \\ \dot{u}_o^{b2} \end{Bmatrix}_l, \begin{Bmatrix} \ddot{u}_o^I \\ \ddot{u}_o^B \end{Bmatrix}_l \equiv \begin{Bmatrix} \ddot{u}_o^{b1} \\ \ddot{u}_o^{b2} \end{Bmatrix}_l \tag{37}$$

They are the outgoing waves and can be obtained as follows.

$$\{u_o^{b1}\}_l = \{u_r^{b1}\}_m - \{u_r^{b1}\}_f \tag{38a}$$

$$\{\dot{u}_o^{b1}\}_l = \{\dot{u}_r^{b1}\}_m - \{\dot{u}_r^{b1}\}_f \tag{38b}$$

$$\{\ddot{u}_o^{b1}\}_l = \{\ddot{u}_r^{b1}\}_m - \{\ddot{u}_r^{b1}\}_f \tag{38c}$$

The non-zero solution of the transmitting-layer is induced only by non-zero boundary values at the boundary nodes b_1, which is obtained by filtering the solution of the main mesh with the solution of the free-field as shown above. The unknown variables solved in the transmitting-layer are nodal displacement, velocity and acceleration on the boundary nodes b_2, i.e. $u_o^{b2}, \dot{u}_o^{b2}, \ddot{u}_o^{b2}$, and they are governed by following equations.

$$\left[M_d^{b2}\right]_l \{\ddot{u}_o^{b2}\}_l + \left[c_{t\_d}^{b2}\right]_l \{\dot{u}_o^{b2}\}_l + \left[K^{b2} + k_t^{b2}\right]_l \{u_o^{b2}\}_l = -[K^{b21}]_l \{u_{ro}^{b1}\}_l \tag{39}$$

These equations can be integrated explicitly with Newmark method. It has been checked that the same free-field motion as that of the free-field column will be obtained in the main mesh with the transmitting-layer boundary model if the main mesh degenerates into the free-field. Once the nodal displacement, velocity and acceleration on the boundary nodes b_2, i.e. $u_o^{b2}, \dot{u}_o^{b2}, \ddot{u}_o^{b2}$, are obtained, we can construct the nodal displacement, velocity and acceleration on the boundary nodes b_2 of the main mesh. The boundary values on the nodes b_2 of the main mesh are as follows.

$$\{u_r^{b2}\}_m = \{u_o^{b2}\}_l + \{u_r^{b2}\}_f \tag{40a}$$

$$\{\dot{u}_r^{b2}\}_m = \{\dot{u}_o^{b2}\}_l + \{\dot{u}_r^{b2}\}_f \tag{40b}$$

$$\{\ddot{u}_r^{b2}\}_m = \{\ddot{u}_o^{b2}\}_l + \{\ddot{u}_r^{b2}\}_f \tag{40c}$$

5.2.5 Computing Procedure

With the above setting of the constituent problems, the actual computing procedure involves all three parts of the structure-foundation mesh simultaneously. Within one computational loop, the following procedure can be identified.

1) Solve Eq. (33) of the main mesh with the displacement of nodes b_2 on the lateral boundary *L-L* and *R-R* prescribed.

$$\{u_r^{b2}\}_m = \{u_o^{b2}\}_l + \{u_r^{b2}\}_f \tag{41}$$

2) Solve Eq. (35) of the free-field columns.

3) Solve Eq. (36) of the transmitting-layers, for the displacement $\{u_o^{b2}\}_l$, with the difference between the main mesh and the free-field column being applied on the boundary nodes b_1.

$$\{u_o^{b1}\}_l = \{u_r^{b1}\}_m - \{u_r^{b1}\}_f \tag{42}$$

4) Obtain the new displacement of boundary nodes b_2 of the main mesh by adding the free-field column solution to the transmitting-layer solution.

$$\{u_r^{b2}\}_m = \{u_o^{b2}\}_l + \{u_r^{b2}\}_f \tag{43}$$

Return back to 1) to initialize the next loop of computation.

The above procedure is simplified in actual computer implementation–the algorithm involves the solution of three problems in parallel (main mesh, free-field columns and transmitting-layers), where the communication of information among the three constituent problems only requires some special sub-procedures. The restriction of material linearity is limited in the transmitting-layer and the foundation layer above the truncated boundary on the bottom. In the interior of the main mesh, arbitrary non-linear material behavior can be accommodated.

6 Numerical Examples

6.1 A Structure-Foundation Subject to Vertically Upgoing Waves

A 2-D structure-foundation subject to vertically upgoing seismic waves is shown in Figure 8, where two models of different sizes have been truncated. The physical and mechanics parameters adopted in this model are shown in table 1. In this paper, all of models adopt the same the physical and mechanics parameters. In the paper, the length and height of the grid are both 10m. For the figure 8, the length and height of small model are 350m and 100m, respectively while the length and height of big model are 390m and 120m, respectively.

Table 1 the physical and mechanics parameters of the model

Density/ρ	Elastic modulus/ E	Poisson's ratio/ μ	Grid size/ h	Time-step/Δt
2×10^3 kg/m^3	2×10^9 Pa	0.20	10 m	0.0080s

In this example, sinusoidal shear and pressure waves have been used to excite the structure-foundation. The results are compared between the small model and the big one. The histories of the stress at sampling point A in the case of shear wave input are shown in Figure 9; and those in the case of pressure wave input are shown in Figure 10.

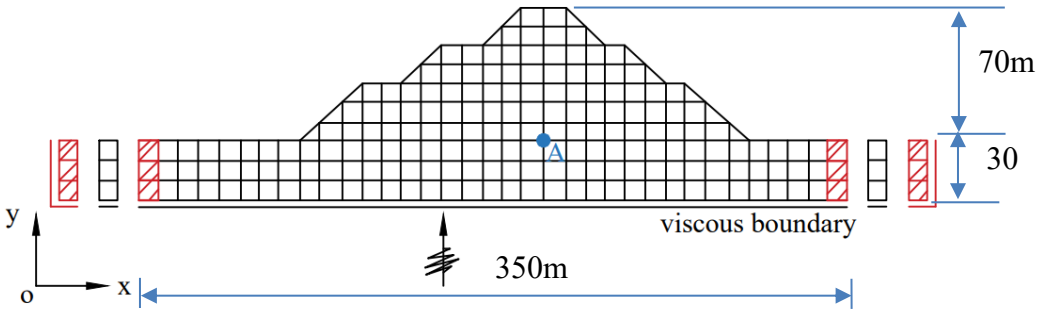

(*a*) *the small model*

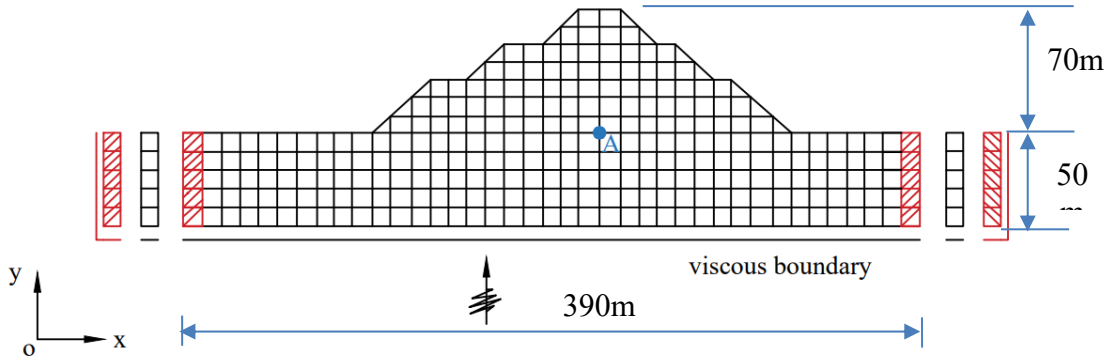

(*b*) *the big model*

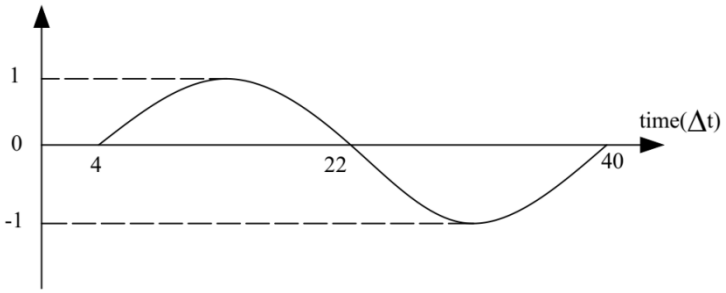

(*c*) *the displacement of the input sinusoidal wave*

Figure 8 *A structure-foundation subject to vertically upgoing plane waves modeled with the transmitting-layer boundary model*

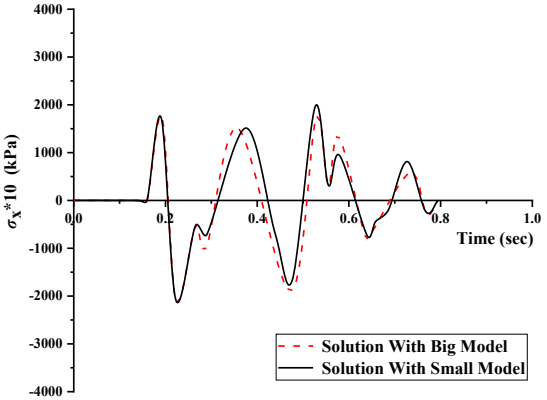

(*a*) σ_x

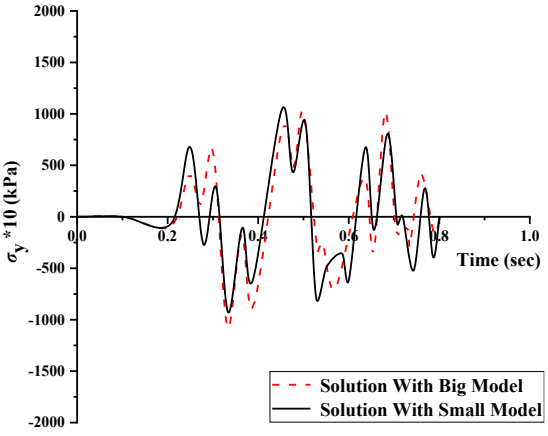

(*b*) σ_y

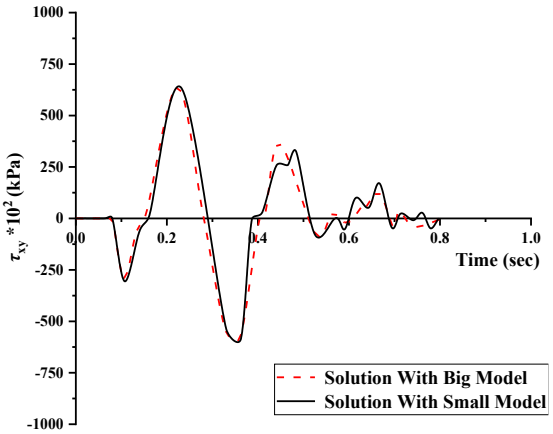

(*c*) τ_{xy}

Note: the sinusoidal wave is used as the upgoing shear wave

Figure 9 *The comparison of stress components at point A between the small mesh and the big mesh*

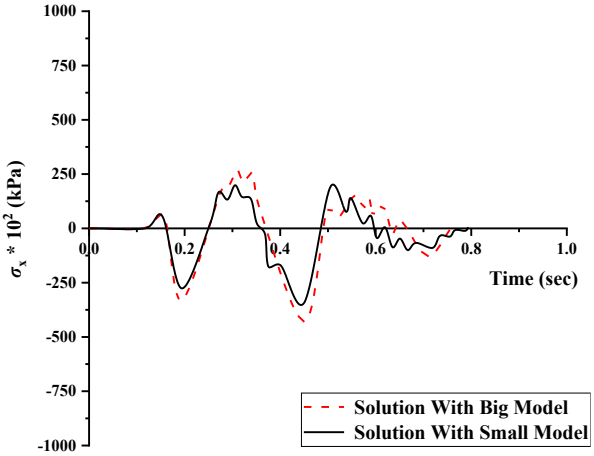

(*a*) σ_x

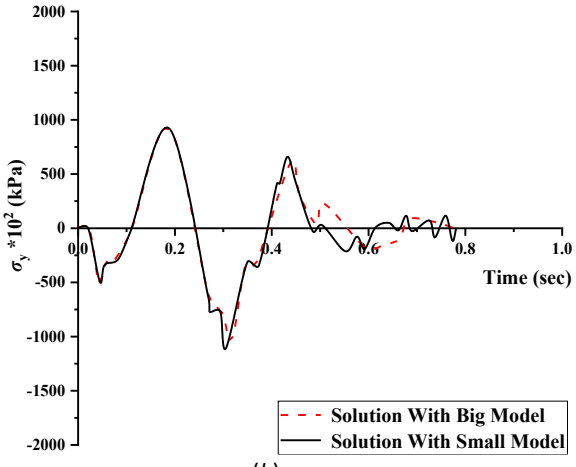

(*b*) σ_y

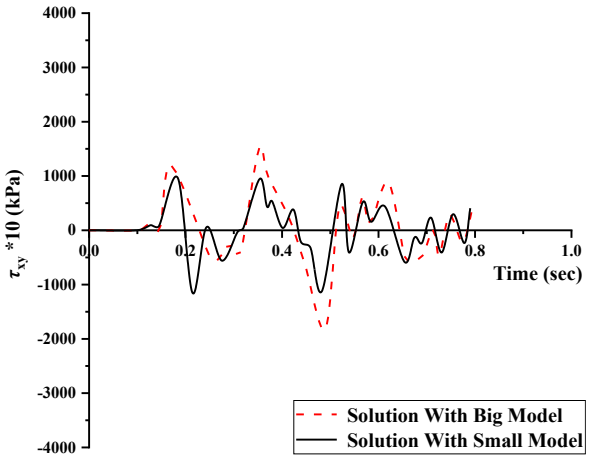

(*c*) τ_{xy}

Note: the sinusoidal wave is used as the upgoing pressure wave

Figure 10 *The comparison of stress components at point A between the small mesh and the big mesh*

In theory, the solution of the small model would be identical to that of the big model exactly if the transmitting boundary worked perfectly. Figure 9~10 show that the general trends of the stress components (σ_x, σ_y and τ_{xy}) between the small model and the big one are consistent with each other. These figures also demonstrate that the stress component amplitudes of the big model are nearly the same with those of the small model. In reality, there might exist a little difference in the solutions between the two models because of numerical dispersion. These differences are within a 5% range, which is acceptable. All of these indicate the correctness and efficiency of the proposed transmitting boundary.

6.2 A Structure-Foundation Subject to Obliquely Incoming Waves

The assumption of plane incoming seismic waves is a good approximation of the earthquake input. For the most structure-foundation problems, the source of a potential earthquake is not necessary directly underneath the structure or the foundation; consequently, the assumption of vertically upgoing waves will not be general enough in practice. The more general case is that the seismic waves approach the structure-foundation obliquely. The tied boundary model is no longer applicable while the transmitting-layer boundary model can be used to handle the problem.

A structure-foundation subject to obliquely incoming waves is illustrated in Figure 11. Two finite element meshes with truncation at different positions are considered for the purpose of comparison study. The incoming seismic waves are assumed to be pressure ones. The parameters adopted in this model are shown in the table 1.

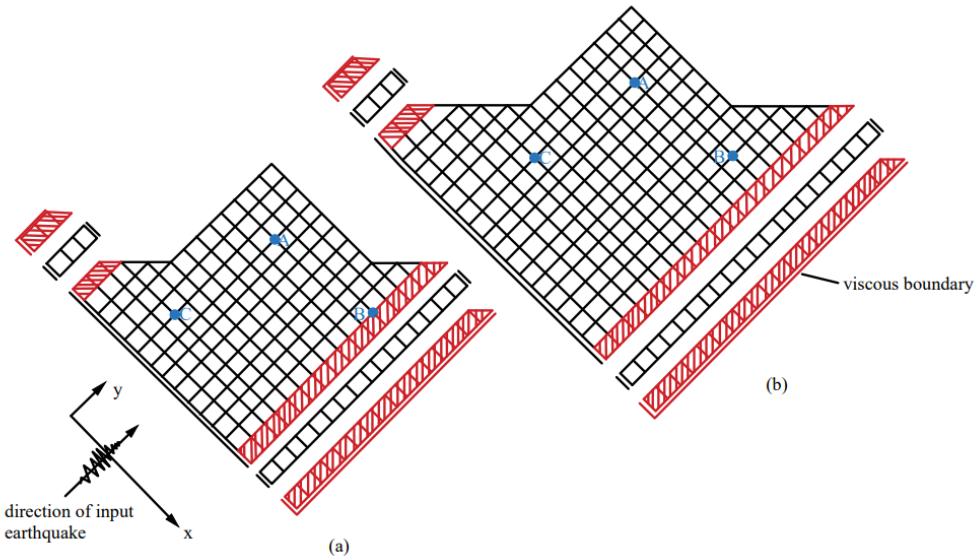

Note: (a) small *mesh* (b) big mesh

Figure 11 *A structure-foundation subject to obliquely incoming plane waves (the transmitting-layer boundary model)*

This problem has been firstly analyzed with the sinusoidal wave input. The stress histories at sampling point A are compared between the small model and the big model in Figures 12.

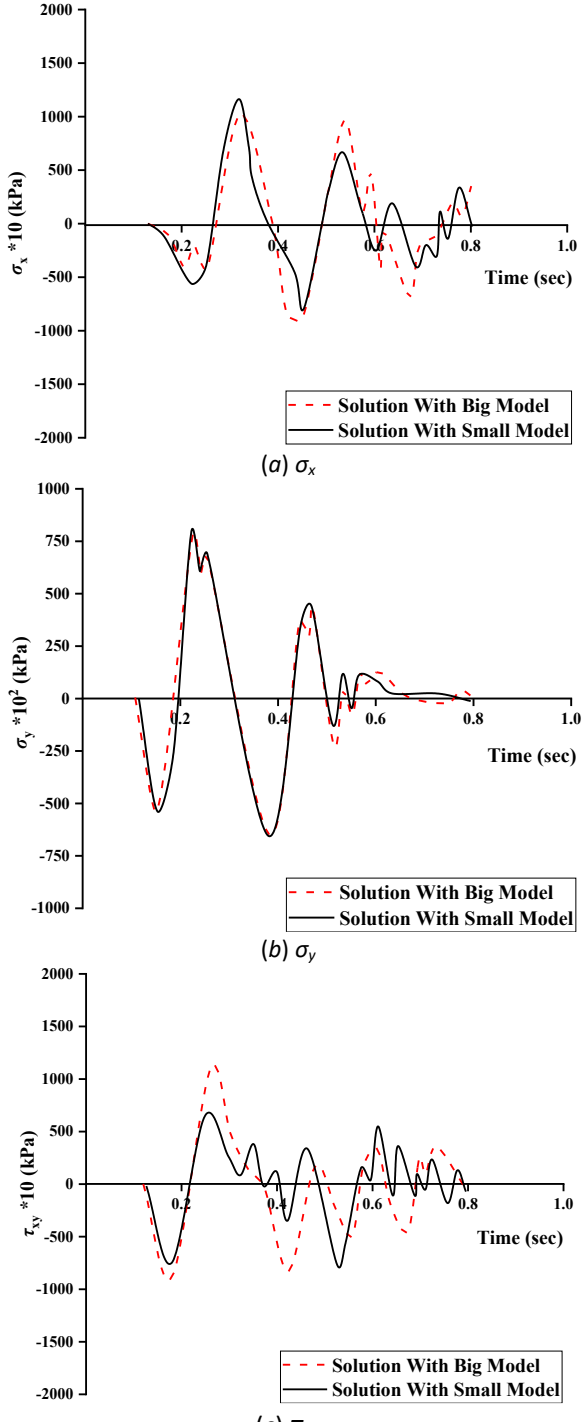

Note: the sinusoidal wave is used as the incoming pressure wave

Figure 12 *The comparison of stress components at point A between the small mesh and the big mesh*

The stress components (σ_x, σ_y and τ_{xy}) at point A of the small model are consistent with those of the big model, so it shows that the transmitting-layer boundary model works correctly and efficiently in the numerical simulation of the structure-foundation under obliquely incoming waves.

The same problem is again analyzed with El Centro seismic input and the results are shown in Figure 13.

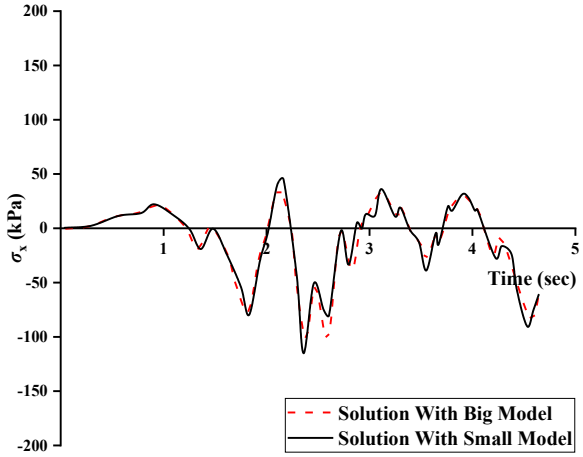

(*a*) σ_x

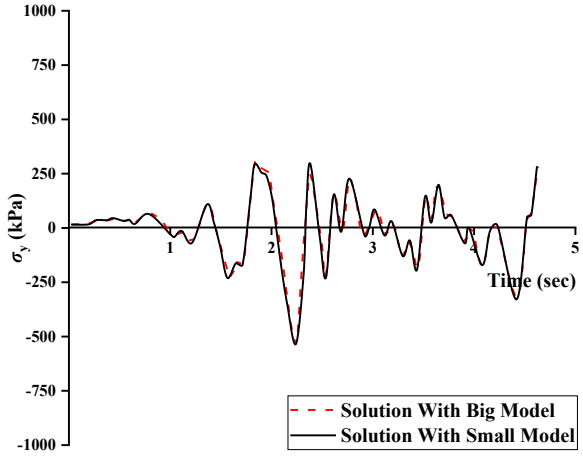

(*b*) σ_y

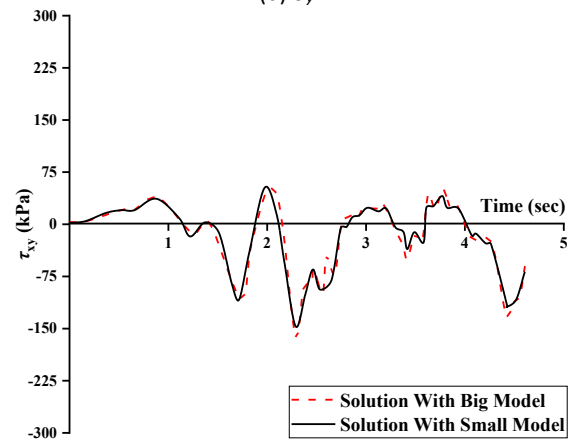

(*c*) τ_{xy}

Note: the El *Centro* seismic record is used as the obliquely incoming pressure waves

Figure 13 *The comparison of stress components at point A between the small mesh and the big mesh*

The quality of the solution of the El Centro seismic input is better than that of the sinusoidal wave input. In this case, the stress components (σ_x, σ_y and τ_{xy}) at point A of the small model are almost identical to those of the big model, so it proves that the transmitting-layer boundary model works correctly and efficiently in the numerical simulation of the structure-foundation subject to obliquely incoming waves.

6.3 A Structure-Foundation Subject to Horizontally Incoming Waves

An extreme case of the obliquely incident earthquake is that the incoming waves approach the structure-foundation horizontally. Although plane body waves cannot propagate along the free surface in theory, the purpose of this assump-

tion is to propose a simple method to approximate the problem of the structure-foundation subject to horizontally incident waves. The tied boundary model is no longer applicable, but the transmitting-layer boundary model can be used to handle this problem.

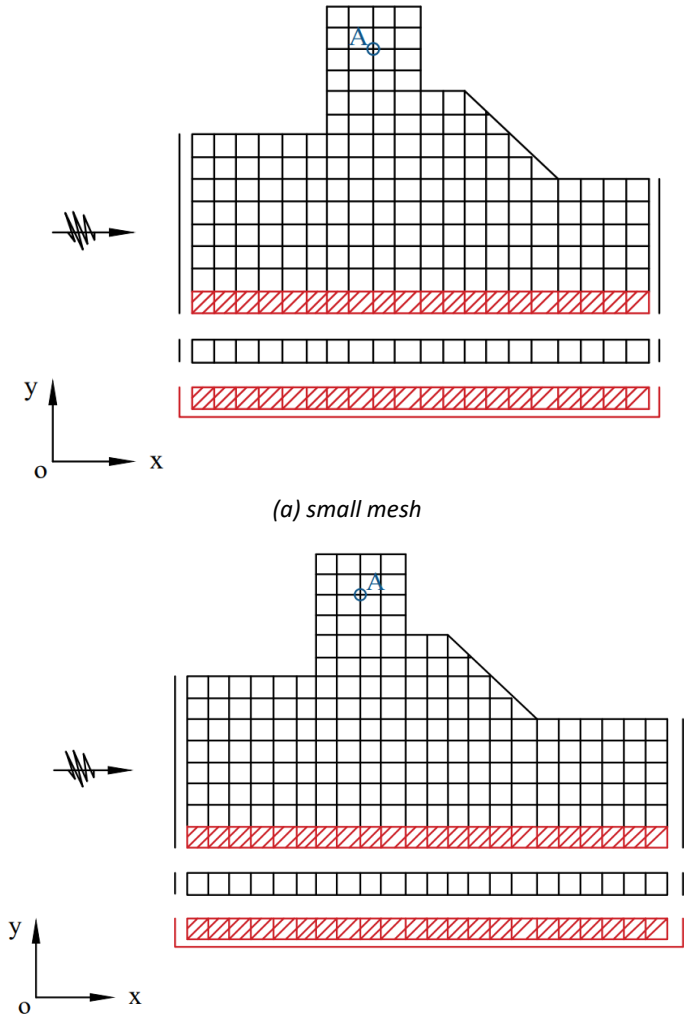

(a) small mesh

(b) big mesh

Figure 14 A structure-*foundation* subject to horizontally incoming waves

An idealized structure-foundation subject to horizontally incoming waves is illustrated in Figure 14. The seismic waves strike the model from the left side of the model. Two meshes with differently truncated boundaries are analyzed for the comparison study. The parameters adopted in this model are shown in the Table 1.

The El Centro seismic record has been chosen as the seismic input. The stress components at the sampling point A are compared between the small model and the big model in Figure 15.

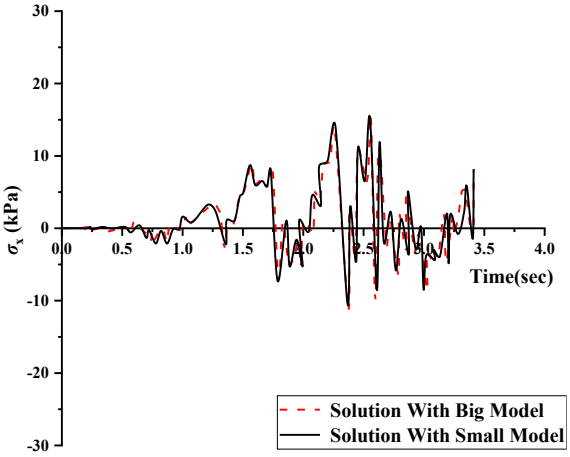

(*a*) σ_x

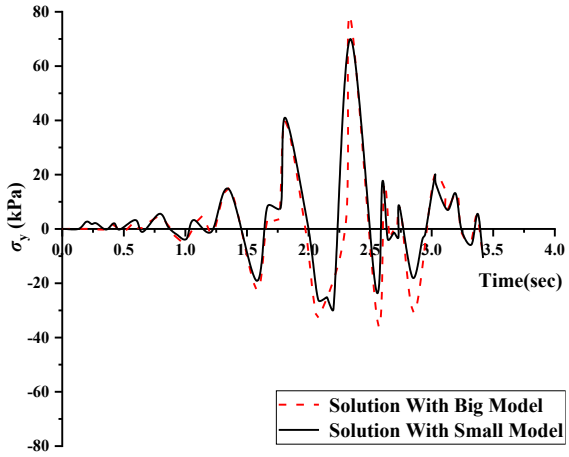

(*b*) σ_y

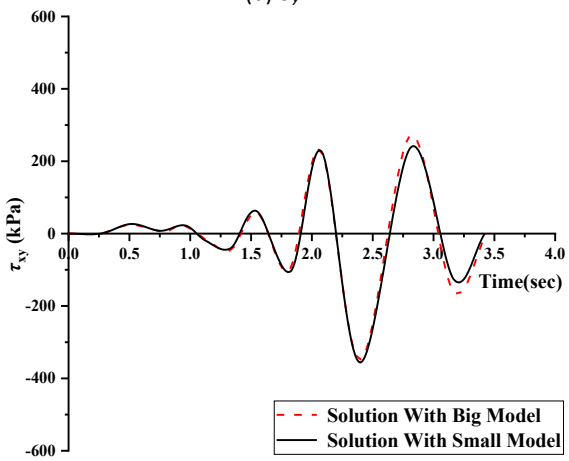

(*c*) τ_{xy}

Note: the El Centro seismic record is used as the horizontally incident pressure wave, μ=0.20

Figure15 *The comparison of stress components at point A between the small mesh and the big mesh*

The stress components (σ_x, σ_y and τ_{xy}) at point A of the small model are almost identical to those of the big model, so it shows that the transmitting-layer boundary model works correctly and efficiently in the numerical simulation of the structure-foundation subject to horizontally incoming waves.

6.4 The Transmitting Boundary Versus the Fixed Boundary

In order to show the difference in the solutions of the transmitting boundary model and those of the conventional fixed boundary model, a finite element model is shown in Figure 16, where the structure-foundation is subjected to vertically upgoing waves. The parameters adopted in this model are shown in the Table 1.

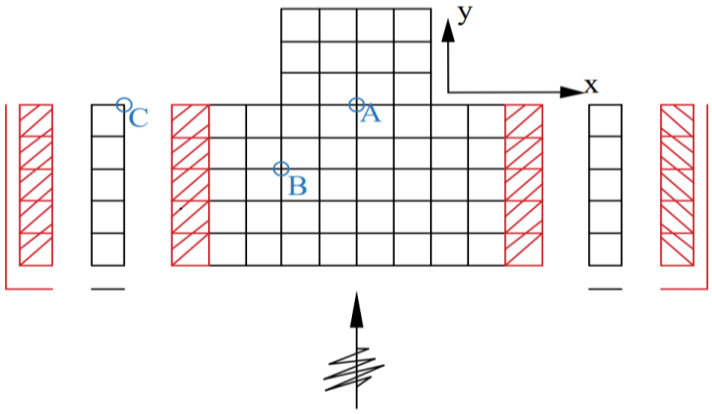

Note: A and B are the sampling point for the structure-foundation and C is the one for free-field

Figure 16 *The Model problem for the comparison study of the two formulations for seismic analysis*

The upgoing pressure wave used in this example is a train of sinusoidal displacement wave, which is shown in Figure 17.

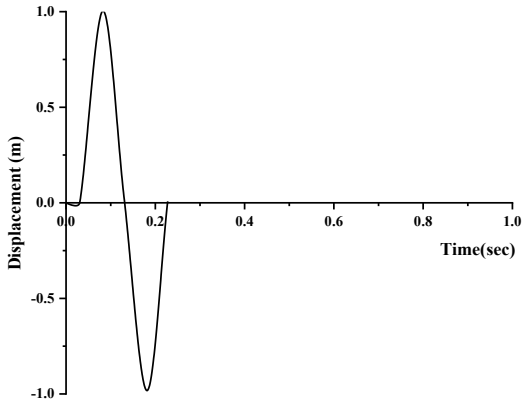

(a) vertical displacement of the incident wave

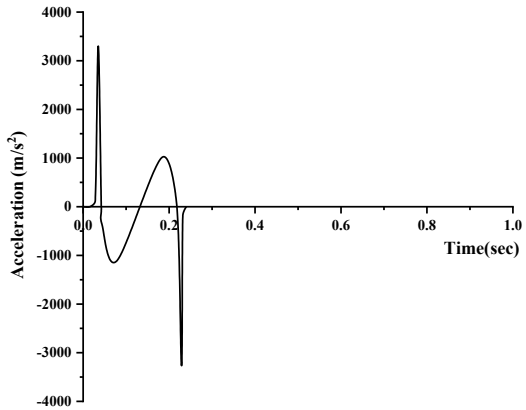

(b) vertical acceleration of the incident wave

Figure 17 *The incident wave chosen for the comparison study*

Firstly, the column of the free-field is analyzed with the formulation of transmitting boundary to get the total motion at the truncated boundary on the bottom. The total displacement and the total acceleration at the bottom boundary are shown in Figure 18, which is used as the total acceleration input in the conventional formulation of the fixed boundary.

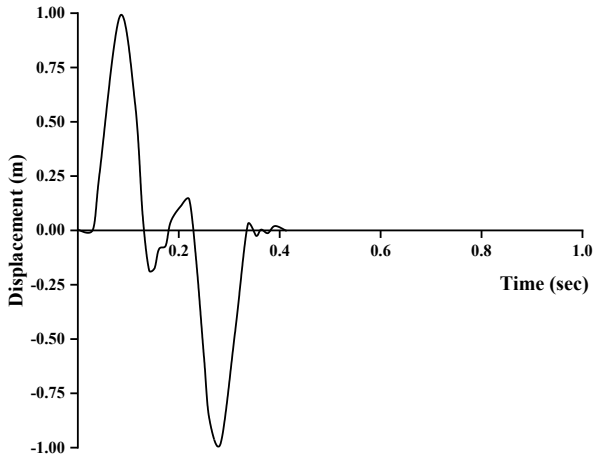

(a) vertical displacement of total motion

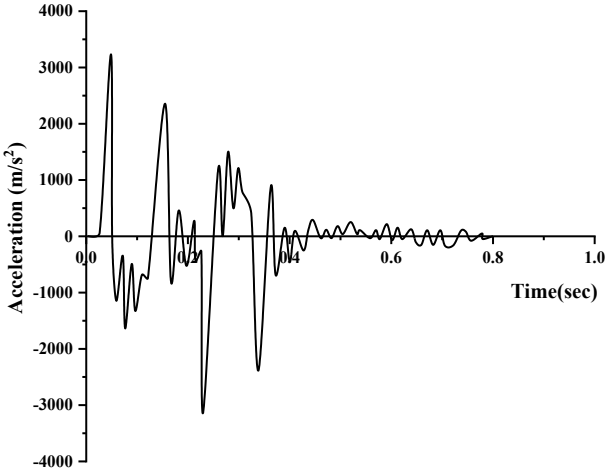

(b) vertical acceleration of total motion

Figure 18 *The motion of the free-field at bottom boundary due to the incident sinusoidal displacement wave*

The numeric results of the free-field obtained with the two formulations are identical and shown in Figure19. The results are further validated by the displacement at the free surface of the free-field, and the displacement is exactly the double of the upgoing displacement wave (Figure 17(a)); it shows that the proposed transmitting boundary is both correct and efficient.

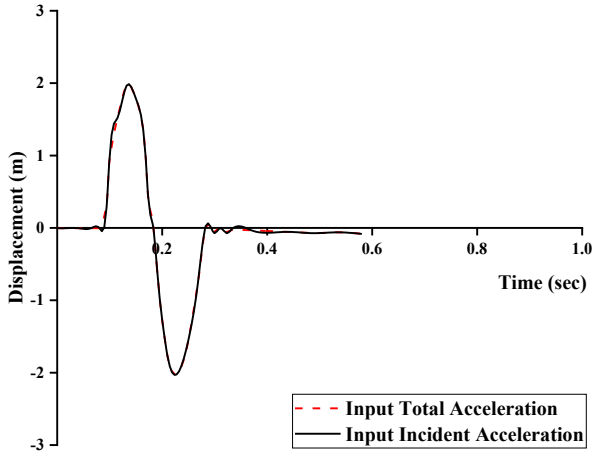

(*a*) *displacement* at ground surface

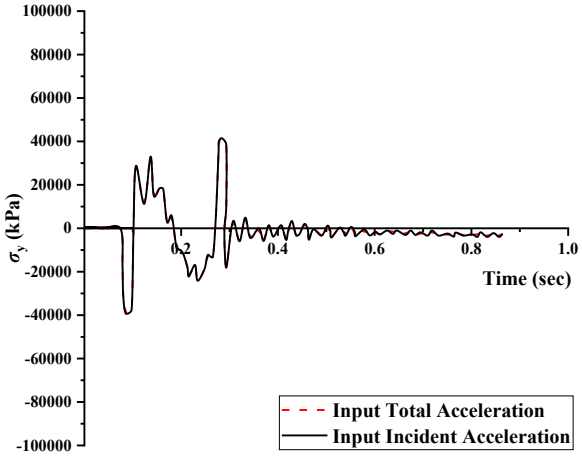

(*b*) *vertically normal stress at position C at the ground surface*

Figure19 *The response of free-field obtained from the two different formulation*

Finally, the structure-foundation problem is analyzed with the two different formulations. The sinusoidal wave shown in Figure 17 is used as the upgoing waves for the formulation of the transmitting boundary, and the total motion of the free-field at the truncated bottom boundary (Figure 18) is used as the seismic input for the formulation of the fixed boundary.

The numeric results are compared in Figures 20-21 between the two different formulations. The vertical displacements (y direction) at the point A and the point B are presented in Figure 20, while the vertically normal stresses (σ_y) are presented in Figure 21.

Obviously, the results (in black solid lines) of the formulation of the transmitting boundary behave as the wave phenomenon, i.e. the structure-foundation will come back to the original equilibrium position when the waves radiate away from the computational model.

It is clearly shown that the traditional formulation of fixed boundary will trap all waves (in red dotted lines) into the interior of the computational model. The reason for the difference is that total motion on the truncated bottom boundary of the structure-foundation problem cannot be known in advance of the formulation of the fixed boundary. Consequently, it is the formulation of the transmitting boundary makes the dynamic interaction of the structure-foundation problem being accounted logically in the formulation itself.

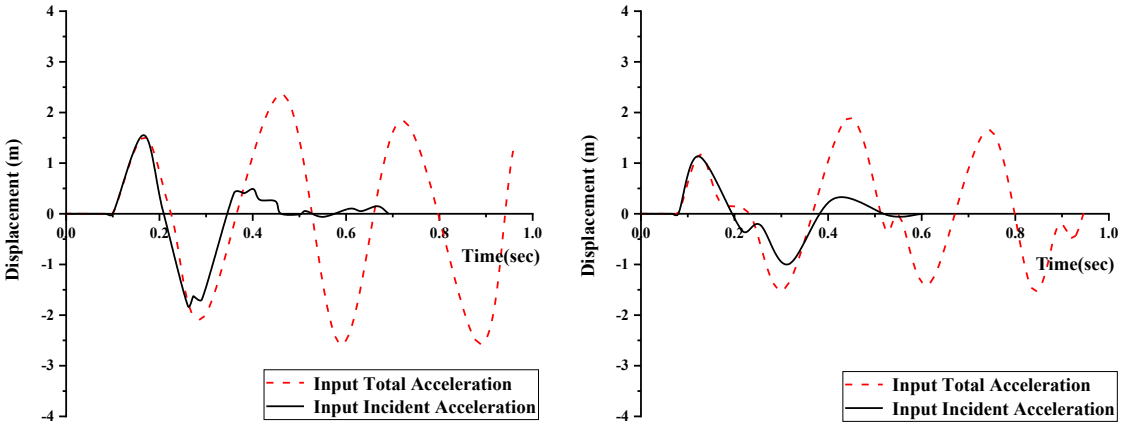

(*a*) *Point A* (*b*) *point B*

Figure 20 *Vertical displacement of the structure-foundation problem*

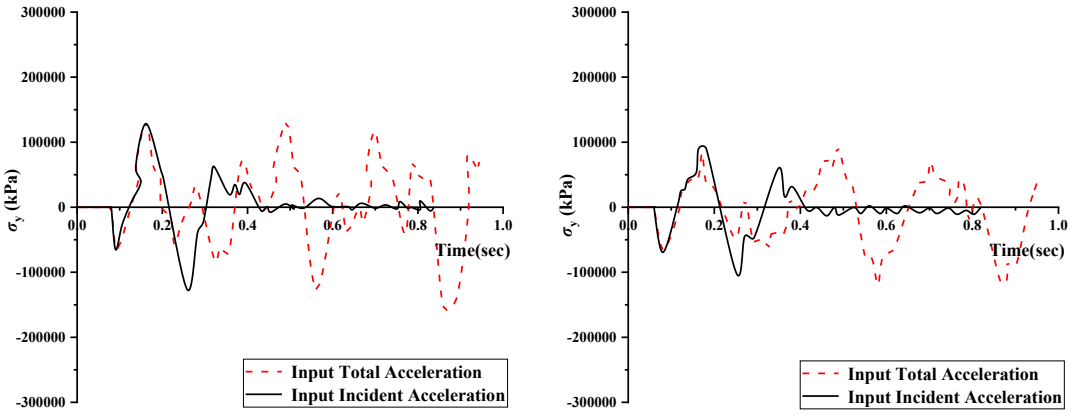

(*a*) *Point A* (*b*) *point B*

Figure 21 *Vertically normal stress of the structure-foundation problem*

This very example proves further that the proposed transmitting boundary is efficient for seismic analysis of the structure-foundation problem.

A critical advantage of the proposed method is its low computational cost. For the model in the Figure16, simulating the fixed boundary case using the full global model requires 2.5 CPU-hours. In contrast, the proposed method, operating only on the significantly smaller localized domain, completed the simulation in 2.7CPU-hours. This efficiency stems primarily from avoiding the repeated solution of the large global system of equations. The localized solve focuses computational effort only on the region experiencing nonlinear effects due to the boundary constraint. This demonstrates a highly favorable accuracy-computational cost trade-off.

As demonstrated in Sections 6.1 ~ 6.4, the test cases include vertical, oblique, and horizontal seismic wave inputs, illustrating the method's adaptability to different wave directions. All models feature irregular geometries, confirming the effectiveness of the proposed transmitting boundaries for such configurations.

Due to space limitations, the efficiency of the transmitting boundary in models with heterogeneous media is not explored here but is addressed in a separate study (Xiong, 2025). In that work, a complex slope model with both irregular geometry and heterogeneous material properties was established. The proposed transmitting boundary was applied to simulate seismic dynamic responses, and the results further verified its efficiency even in heterogeneous media.

7 Conclusions

The purpose of this paper is to study the transmitting boundary and to develop finite computational models for seismic analysis of the structure-foundation. Now some general conclusions can be summarized as follows.

The modified viscous boundary has the stiffness-like terms in the boundary conditions to address the non-plane wave behavior. The standard viscous boundary is a special case of the modified boundary.

Using incoming seismic waves as the seismic input and imposing the transmitting boundary conditions at the artificially truncated boundary, the dynamic interaction of the structure-foundation can be addressed for non-linear analysis with the formulation of the transmitting boundary model.

Two transmitting boundary models have been developed for seismic analysis of the structure-foundation and they are the tied boundary model and the transmitting-layer boundary model. In the formulation of the transmitting-layer boundary model, the linearity is only required in the vicinity of the truncated boundary of the system. And the transmitting-layer boundary model is more efficient and versatile than the tied boundary model. The transmitting-layer boundary model can also be extended to address dynamics of the structure-foundation subject to obliquely and horizontally incoming seismic waves.

The main limitation is assuming linearity near boundaries. This enables robust, efficient solutions for many problems but restricts use to systems where nonlinearities are away from key boundaries.

Acknowledgements

We extend our deepest thanks to the Institute of Engineering Mechanics, CEA, for providing the strong-motion data. This research work was supported by the National Natural Science Foundation of China (Grant No. 42107173), the Natural Science Foundation of Anhui Province (Grant No. 2108085ME190) and the Fundamental Research Funds for the Central Universities.

Author Contributions: Feng Xiong contributed to the study conception and design. Material preparation, data collection and analysis were performed by Fengqiang Shen and Feng Xiong. The first draft of the manuscript was written by Feng Xiong and all authors commented on previous versions of the manuscript. All authors read and approved the final manuscript.

Editor: Pablo Andrés Muñoz Rojas

References

Amorosi, A., Boldini, D., (2009). Numerical Modelling of the Transverse Dynamic Behaviour of Circular Tunnels in Clayey Soils. Soil Dynamics and Earthquake Engineering 29: 1059-1072.

Barros, G., Pereira, A., Rojek, J., et al., (2024). Time domain coupling of the boundary and discrete element methods for 3D problems[J].Computational Mechanics 74(4):779-797.

Bazyar, M., Song, C., (2017). Analysis of Transient Wave Scattering and its Applications to Site Response Analysis Using the Scaled Boundary Finite-Element Method. Soil Dynamics and Earthquake Engineering 98: 191-205.

Chen, G.X., Jin, D.D., Zhu J, Shi J, Li X.J., (2015). Nonlinear Analysis on Seismic Site Response of Fuzhou Basin, China. Bulletin of the Seismological Society of America, 105: 928-949.

Chen, L., Li, B., Li, P., (2024). 1-D Finite Element Artificial Boundary Method for Saturated Layered Half-Space Site Response under Obliquely Incident P-SV Waves[J].KSCE journal of civil engineering 28(1):169-185.

Cui, F., Chen. Y., Zhang, Y., et al., (2021). Research on application of ground penetrating radar array method based on plane beam signal in different geological models. Acta Geophysica. 69: 2241–2260.

Farhad, A. A. A., Aydn, E., (2025). Viscous Damper Optimization in Low-Rise Adjacent Buildings Exposed to Earthquakes by Considering the Soil-Structure Interaction. Buildings 15(2):260.

Fattah, M. Y., Hamood, M. J., Dawood, S. H., (2015), Dynamic Response of a Lined Tunnel with Transmitting Boundaries. Earthquakes and Structures 8 (1): 275-304.

Fattah, M. Y., Schanz, T., Dawood, S. H., (2012a), The Role of Transmitting Boundaries in Modeling Dynamic Soil-Structure Interaction Problems. International Journal of Engineering and Technology 2012, 2(2): 236-258.

Fattah, M. Y., Shlash, K. T., al-Soud, M. S., (2012b), Boundary Element Analysis of a Lined Tunnel Problem. International Journal of Engineering, IJE TRANSACTIONS B: Applications 25(2):87-94.

Guo, Z., Zhang, Z., Yuan, Y., (2024). Seismic soil pressures on underground metro station in soft soil: Experimental studies and analytical comparisons. Soil dynamics and earthquake engineering 176(1):108334.1-108334.12.

Hashash, Y.M.A., Karina, K., Koutsoftas, D., O'Riordan, N., (2010). Seismic Design Considerations for Underground Box Structures. American Society of Civil Engineers (ASCE) 3: 620-637.

Han, S., Sun, J. & Xiong, F., (2025). Analysis for site seismic hazard probability considering the orientation distribution of potential seismic sources. Natural Hazards 121(3): 2433-2464.

Huang, J.Q., Du, X.L., Jin, L., Zhao, M., (2016). Impact of Incident Angles of P Wave on the Dynamic Responses of Long Lined Tunnels. Earthquake Engineering and Structural Dynamics 45: 2435-2454.

Huang, J.Q., Du, X.L., Zhao, M., Zhao, X., (2017). Impact of Incident Angles of Earthquake Shear (S) Waves on 3-D Non-Linear Seismic Response of Long Lined Tunnels. Engineering Geology 222: 168-185.

Kim, D. and Yun, C.B., (2015). Time-domain Soil-Structure Interaction Analysis in Two-Dimensional Medium Based on Analytical Frequency-Dependent Infinite Elements. International Journal for Numerical Methods in Engineering 47: 1241-1261.

Kumar A., Kapuria S., (2022). Finite Element Simulation of Axisymmetric Elastic and Electroelastic Wave Propagation Using Local-Domain Wave Packet Enrichment. Journal of Vibration and Acoustics 144(2):12.

Lan F., Guo T., (2024). Non-monotonic dynamics (mixed hardening/softening) in nonlinear continuous structures: An asymptotic formulation.Nonlinear Dynamics 112(17):14745-14772.

Liao, Z.P., Huang, K.L., Yang, B.P., Yuan, Y.F., (1984). A Transmitting Boundary for Transient Wave Analyses. Science in China Series A 27: 1063-1076.

Liu, J.B., Du, Y.X., Du, X.L., Wang, Z.Y., Wu, J., (2006). 3D Viscous-Spring Artificial Boundary in Time Domain. Earthquake Engineering and Engineering Vibration 5: 93-102.

Liu, J.B., Lu, Y.D., (1998). A direct method for analysis of dynamic soil-structure interaction based on interface idea. Developments in Geotechnical Engineering 83: 261-276.

Lysmer, J. and Kuhlemeyer, R.L., (1969). Finite Dynamic Model for Infinite Media, Journal of the Engineering Mechanics Division, ASCE 95: 859-877.

Nielsen, A.H., (2014). Towards a Complete Framework for Seismic Analysis in Abaqus. Proceedings of the ICE-Engineering and Computational Mechanics 167: 3-12.

Pan, J.W., Zhang, C.H., Wang, J.T., Xu, Y.J., (2014). Seismic Damage-Cracking Analysis of Arch Dams Using Different Earthquake Input Mechanisms. Science in China Series E 52: 518-529.

Pitilakis, K., Tsinidis, G., (2010). Seismic Design of Large, Long Underground Structures: Metro and Parking Stations, Highway Tunnels. International Geotechnical Conference geotechnical Challenges of Megacities, Geomos.

Shen, F.Q. (1988). Transmitting Boundary in Dynamic Computation, PhD Thesis, C/PhD/107/88, University College of Swansea.

Wang, H.W., (2024). Amplitude and phase approximation at the linear slip interface of two different tilted transversely isotropic media. Acta Geophysica, 72: 2297–2314.

Wolf, J.P., (1988). Soil-Structure Interaction Analysis in Time Domain. Nuclear Engineering and Design, 111: 381-393.

Tirri A., Nitti A., Sierra-Ausin J., et al., (2023). Linear stability analysis of fluid–structure interaction problems with an immersed boundary method. Journal of Fluids and Structures, 117:103830.

Xia, Y., Wu. W., Jiao, Y. , et al., (2025). Numerical investigation of wave propagation across rock masses through a nodal-based 3D discontinuous deformation analysis method with contact potential. Engineering Analysis with Boundary Elements 172(3):106120.

Xiong, F., Sun, J., Qi, S. Shao A.Y., Han S.C., (2025). Critical peak acceleration characteristics of a slope against actions of P and S waves with different incident directions. Acta Geophysica 73(4):3159-3175.

Xu, C.S., Song, J., Du, X.L., Zhao, M., (2017). A Local Artificial-Boundary Condition for Simulating Transient Wave Radiation in Fluid-Saturated Porous Media of Infinite Domains. International Journal for Numerical Methods in Engineering 112: 529-552.

Xu, Q., Chen, J.Y., Li, J., Fan, S.L., (2012). New Artificial Boundary Condition for Saturated Soil Foundations. Earthquake Engineering and Engineering Vibration 11: 139-147.

Zhao, M., Wu, L.H., Du, X.L., Zhong, Z.L., Xu, C.S., Li, L., (2018). Stable High-Order Absorbing Boundary Condition Based on New Continued Fraction for Scalar Wave Propagation in Unbounded Multilayer Media. Computer Methods in Applied Mechanics and Engineering 334: 111-137.

Zhang, C.H., Pan, J.W., Wang, J.T., (2014). Influence of Seismic Input Mechanisms and Radiation Damping on Arch Dam Response. Soil Dynamics and Earthquake Engineering 29: 1282-1293.

Zienkiewicz, O.C., Bicanic, N., Shen, F.Q., (1989). Earthquake Input Definition and the Transmitting Boundary Conditions, Chapter 3, Advances in Computational Nonlinear Mechanics (edited by I. St. DOLTSINIS), Springer-Verlag.

Zienkiewicz, O.C., Taylor, R.T., Zhu, J.Z., (2005). The Finite Element Method: Its Basis and Fundamentals. The Sixth Edition, Linacre House, Jordan Hill, Oxford OX2 8DP: Elsevier Butterworth-Heinemann.